J Solid State Eletrochem (2004) 8: 505–510
DOI 10.1007/s10008-003-0465-x

ORIGINAL PAPER

Guoliang Chen · Dennis E. Tallman
Gordon P. Bierwagen

Unusual microstructures formed during the mediated electrodeposition of polypyrrole on Al 2024-T3 at low current densities

Received: 30 July 2003 / Accepted: 2 October 2003 / Published online: 13 December 2003

Abstract We have recently described the direct electrodeposition of polypyrrole on aluminum alloy 2024-T3 using electron transfer mediation. While studying the nucleation and growth phases of this deposition process using atomic force microscopy, we observed the formation of unusual polypyrrole structures. These structures formed only at low current density (10–100 μA/cm^2), only in the presence of the mediator (4,5-dihydroxy-1,3-benzenedisulfonic acid disodium salt), and only in cells employing a small-area counter electrode (relative to the working electrode area). In this report, we present some of these interesting polypyrrole structures and the conditions of their formation.

Keywords Electrodeposition · Electron transfer mediation · Polypyrrole structures

Introduction

Our group has been exploring various conjugated polymers (such as polyaniline, polypyrrole, and polythiophene) for use as corrosion control coatings, particularly for aluminum alloys [1, 2, 3, 4, 5]. One factor that limits the application of conjugated polymers (CPs) as corrosion control coatings is the difficulty in casting such polymers as films or coatings, since most conjugated polymers are insoluble in environmentally friendly solvents unless suitably derivatized. The direct electrodeposition of CPs onto aluminum and its alloys is generally not feasible owing to the positive potentials required for polymerization, potentials at which the metal oxidizes (corrodes) and an adherent, continuous film is difficult to achieve.

We have developed an approach that uses electron transfer mediation to reduce the deposition potential of polypyrrole (Ppy) on aluminum and aluminum alloy by nearly 500 mV, permitting film deposition from aqueous solution with nearly 100% current efficiency [6, 7, 8]. The mediator used most often in this work is 4,5-dihydroxy-1,3-benzenedisulfonate, or Tiron, which can also serve as the dopant or counter ion in the polymer, but other mediators appear promising [8]. Galvanostatic electrodeposition of Ppy in the presence of Tiron leads to uniform, adherent, conducting, electroactive films.

In an attempt to better understand the role of Tiron in the mediation process, we undertook electrochemical atomic force microscopy (ECAFM) studies. The AFM images in combination with the potential–time curves obtained during galvanostatic electrodeposition of Ppy at 0.5 mA/cm^2 indicated that Tiron mediated both the initial nucleation event (initial Ppy deposition on the Al/Al_2O_3 surface) and the film growth stage (Ppy deposition on Ppy) [6, 9]. Many more nucleation sites were observed in the presence of Tiron than in control experiments where Tiron was replaced by sodium *p*-toluenesulfonate (pTS) [9]. Furthermore, the maximum potential reached in the presence of Tiron during both the nucleation stage and the film growth stage was several hundred millivolts less positive than that observed in the control experiments (with pTS) [6].

The ECAFM experiments described previously [9] were conducted at a constant current of 0.5 mA/cm^2 to approximate the conditions under which we typically grow the Ppy films [6, 7, 8]. To slow down the deposition process in order to obtain better images of the very earliest stages of deposition, more recent experiments described here were performed at current densities in the range 10–100 μA/cm^2. It was under these low current conditions that we first observed unusual polymer structures. In this paper, we describe the influence of

G. Chen · D. E. Tallman (✉)
Department of Chemistry,
North Dakota State University,
Fargo, ND , 58105-5516, USA
E-mail: dennis.tallman@ndsu.nodak.edu
Tel.: +1-701-2318696
Fax: +1-701-2318439

D. E. Tallman · G. P. Bierwagen
Department of Polymers and Coatings,
North Dakota State University, Fargo,
ND, 58105-5516, USA

current density, electrolyte, electrochemical cell geometry, and pH on the morphology of the deposited polymer structures.

Experimental

Materials

Pyrrole (Aldrich Chemical Company, Inc) was freshly distilled under reduced pressure. Tiron (Aldrich) or pTS was used as supporting electrolyte and Milli-Q water was used as solvent. The electrodes were Al 2024-T3 (Q-Panel) and were prepared for electrodeposition by dry-polishing to 1500 grit followed by rinsing with hexane. All chemical reagents used were analytical grade.

Atomic force microscopy

A Nanoscope III scanning probe microscope (Digital Instruments, Santa Barbara, Calif.) with a J scanner (125 μm cantilever with a maximum scan size of 153 μm) was used for all AFM and ECAFM experiments. The imaging was performed in the contact mode. The optical micrographs were captured from the video microscope unit of the AFM.

Scanning electron microscopy and energy dispersive spectroscopy

Scanning electron microscopy (SEM) was performed using a JEOL JSM 6300 scanning electron microscope (JEOL, Boston, Mass.). Samples were mounted on aluminum stubs with silver glue. The specimens were coated with gold-palladium in a Balzers SCD-030 sputter coater. The microscope was operated at 10^{-7} Torr and 15 kV. Elemental analysis was obtained by energy dispersive X-ray spectroscopy (EDS) via a ThermoNoran EDS detector.

Electrodeposition

Electrodeposition solutions typically contained 0.1 M pyrrole and either 0.1 M Tiron or 0.1 M pTS at pH 3 (adjusted with dilute sulfuric acid), unless noted otherwise. Electrodepositions were performed in two different cells. For electrodepositions performed in situ while imaging by AFM, the standard three-electrode electrochemical cell supplied for the Nanoscope III was used (Digital Instruments), with a cell volume of approximately 0.055 cm^3. A disk of Al 2024-T3 having an exposed area of 1.77 cm^2 served as the working electrode, a platinum wire (length 0.25 cm, diameter 94 μm) as the counter electrode, and a silver wire (diameter 141 μm) as the reference electrode. These ECAFM experiments were performed in the galvanostatic mode and the potential was monitored throughout the deposition.

The ECAFM cell described above is poorly designed for electrodeposition, a consequence of the mismatch in working and counter electrode areas (the working electrode is much larger) and the placement of electrodes within the cell (the wire counter electrode is off to one side of the working electrode). In order to ascertain the influence of this unfavorable cell geometry on the observed results, electrodepositions were also performed in a large-volume (ca. 100 cm^3) three-electrode cell using an EG & G model 273A potentiostat/galvanostat (EG & G Princeton Applied Research). This cell included an Al 2024-T3 working electrode (3-cm×3-cm plate) and a saturated Ag/AgCl reference electrode. Either a platinum wire (length 4 cm, diameter 94 μm) or a platinum plate (4-cm×3-cm) was used as the counter electrode. In experiments with this cell, the current density during various electrodepositions was controlled at values ranging from 100 $\mu A/cm^2$ to 1.2 mA/cm^2.

Results and discussion

Polypyrrole films produced by ECAFM at high current density

First, we note that Ppy films produced in our ECAFM cell at high current density ($>500\ \mu A/cm^2$) have a morphology similar to those reported earlier on active metals such as steel [10] and aluminum [9, 11] and on noble metals such as platinum and gold [12]. Figure 1 shows SEM and AFM images of an air-dried Ppy film formed by an 8-min Tiron-mediated electrodeposition (in the ECAFM cell) on Al 2024-T3 at a current density of 750 $\mu A/cm^2$. The film exhibits the usual nodular or cauliflower-like morphology. Closer inspection reveals that the larger nodules are built from sphere-like nanoparticles, the diameters of which are 100–200 nm [13]. When Tiron (a mediator) was replaced by pTS (a non-mediator), electrodeposition of Ppy was slow and patchy and occurred at more positive potentials. The Ppy that did deposit under these conditions exhibited the nodular morphology similar to that of Fig. 1.

At current densities greater than 500 $\mu A/cm^2$, the mediated Ppy formation/deposition was very fast on the AFM time scale, and it was very difficult to obtain in situ images after about 5 min. Some of the rather

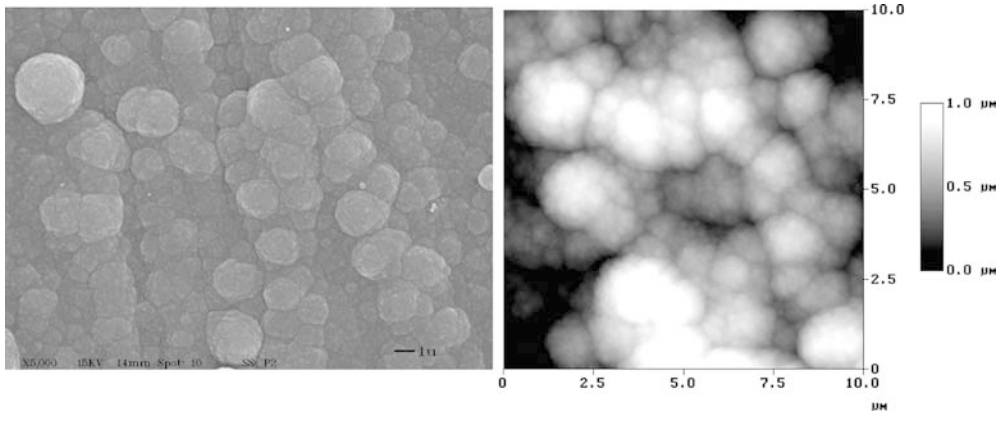

Fig. 1 SEM (*left*) and AFM (*right*) images of an air-dried polypyrrole film formed by an 8-min Tiron-mediated electrodeposition in the ECAFM cell on Al 2024-T3 at a current density of 750 $\mu A/cm^2$. The deposition solution contained 0.1 M pyrrole and 0.1 M Tiron at pH 3

opaque polymerization products (oligomers and polymers) remained suspended in the solution and dispersed throughout the electrochemical cell (as observed with the video microscope), interfering with the AFM laser signal and increasing the imaging noise. Thus, the 8-min image of Fig. 1 was obtained ex situ (in air) after the deposited polymer was rinsed and dried. We also note here that Ppy electrodepositions performed in larger volume cells with optimized (i.e., parallel) placement of working and counter electrodes did not result in significant formation of suspended polymer/oligomer material [6]. We conclude that the unfavorable ECAFM cell geometry (with its high ratio of working electrode area to volume and a poor electrode arrangement) was responsible for such differences in deposition behavior at high current density.

Polypyrrole structures produced by ECAFM at low current density

To obtain better time-resolved AFM images and to circumvent the laser signal problem described above, the Ppy formation/deposition rate was reduced by employing a lower deposition current. At a current density of 50 μA/cm^2, images could be acquired for up to 60 min, after which time the reflected laser signal became obscured by suspended polymer products in solution. The in situ AFM image acquired after a 55-min deposition at 50 μA/cm^2 revealed numerous very small nodules of deposited Ppy on the alloy surface (Ppy deposition was also confirmed by visual observation using the video microscope). However, when these samples were rinsed in Milli-Q water, air-dried for 48 h and then imaged in air (the same procedure used for ex situ AFM imaging in the preceding section), interesting fiber-like structures were observed (Fig. 2). The existence of the fibers was confirmed in SEM images (also Fig. 2). These fiber-like structures were not observed in the high current density images of the preceding section, nor were they observed when Tiron was replaced by pTS (in fact, no polymer formation at all was observed with pTS at current densities below 100 μA/cm^2). The in situ observation of these fiber-like structures by AFM was likely mitigated by their ability to be moved about by the AFM tip during contact mode imaging. Only after the sample was rinsed and dried were the fibers sufficiently anchored to the surface to permit AFM imaging. In many cases the fibers appeared to be suspended at varying heights above the substrate surface (Fig. 2). From SEM images, it was estimated that approximately 90% of the sample area was covered by fibers.

The fibers appear to form more or less radially from a nucleation site, as shown in the SEM image of Fig. 3. The high-resolution AFM image of the fibers in Fig. 3 reveals that they possess a very smooth surface texture, perhaps suggesting a crystalline form of the polymer. Under an optical microscope, these fibers exhibited the dark blue-black appearance characteristic of polypyrrole.

To verify that the fibers were indeed polymer, energy dispersive X-ray spectroscopy (EDS) was performed to obtain their elemental composition. Four analyses were performed on selected fibers, and four analyses were performed on the underlying surface. Of particular interest here are the results for carbon, oxygen, nitrogen, sulfur, aluminum, and copper, summarized in Table 1. First we note that the C, N, and S percentages of the fibers are consistent with Tiron-doped Ppy. The off-fiber results show significantly lower C and N, higher Al, O and Cu, and similar S, consistent with a surface of aluminum alloy and its oxide, partially covered by very small nodules of Ppy as described earlier in this section. The similar sulfur content may also reflect the propensity of 1,2-dihydroxybenzene compounds such as Tiron to adsorb onto aluminum alloy surfaces [8].

Two additional control experiments were performed at low current density to dispel our concerns that the observed fiber structures might somehow be artifacts of the sample preparation and/or imaging procedures. In one control experiment, the exact same procedure as described above was performed, except that pyrrole was omitted from the electrodeposition solution. Current at 50 μA/cm^2 was passed for various lengths of time (up to 120 min) and the samples were prepared for SEM and ex situ AFM imaging exactly as before. Neither the nodular

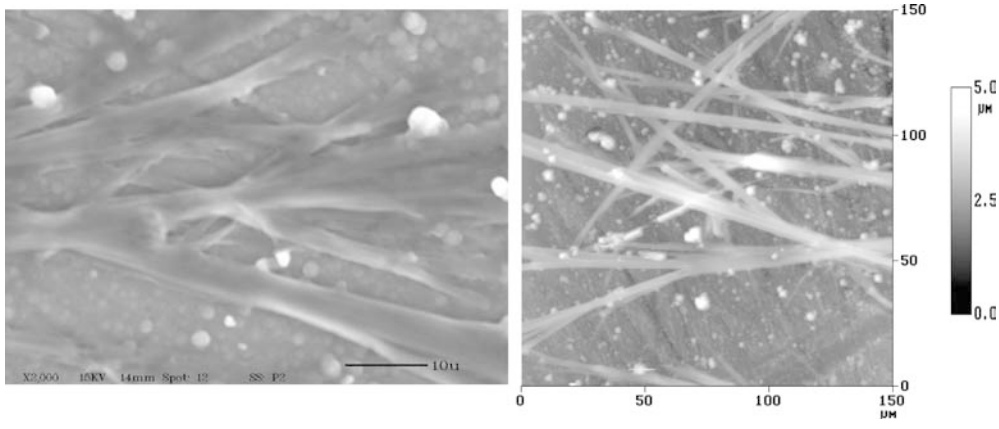

Fig. 2 SEM (*left*) and AFM (*right*) images of air-dried polypyrrole fiber-like structures formed by a 55-min Tiron-mediated electrodeposition in the ECAFM cell on Al 2024-T3 at a current density of 50 μA/cm^2. The deposition solution contained 0.1 M pyrrole and 0.1 M Tiron at pH 3

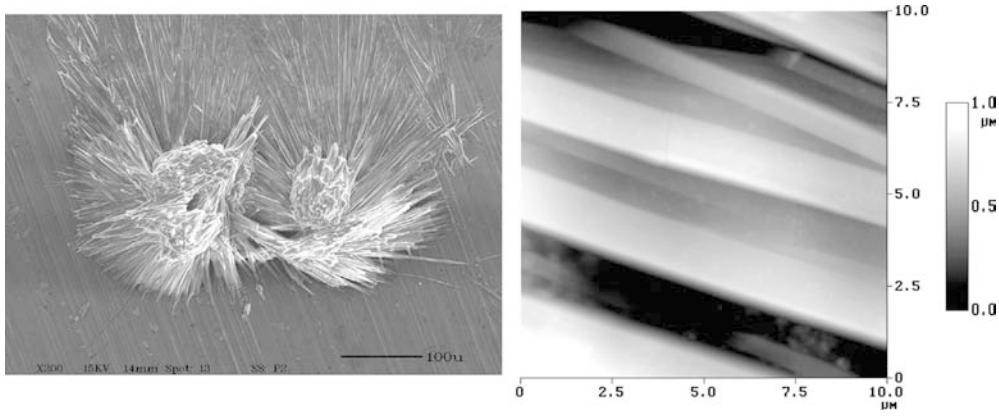

Fig. 3 SEM (*left*) and AFM (*right*) images of air-dried polypyrrole fiber-like structures formed by a 55-min Tiron-mediated electrodeposition in the ECAFM cell on Al 2024-T3 at a current density of 50 μA/cm^2. The deposition solution contained 0.1 M pyrrole and 0.1 M Tiron at pH 3

Table 1 Average atom percent of the various elements on-fiber and off-fiber

Location	C	O	N	S	Al	Cu
On-fiber	61 ± 1	11 ± 1	10 ± 1	11.1 ± 0.4	6.3 ± 0.5	0.03 ± 0.05
Off-fiber	28 ± 2	29 ± 2	2.6 ± 0.5	12 ± 1	12.9 ± 0.5	2.4 ± 1.0

nor the fiber structures were observed in this control experiment. In the other control experiment, pTS replaced Tiron, all other conditions remaining the same. Here again, neither nodular nor fiber structures could be detected for applied current densities of 50 μA/cm^2 and 100 μA/cm^2. Only at ca. 1 mA/cm^2 and above could Ppy deposition be observed in a reasonable time (under 1 h), and the rinsed and air-dried deposit exhibited a nodular structure similar to that of Fig. 1. We conclude that application of low current density (i.e., a slow polymerization rate) combined with electron transfer mediation by Tiron are necessary for the formation of the Ppy fiber-like structures. Additionally, the very non-uniform current distribution which most certainly exists in the ECAFM cell may also play a role in the formation of these unusual structures. Furthermore, the small volume of the ECAFM cell (or more specifically, the small ratio of cell volume to working electrode area) used in these experiments almost certainly leads to a pH decrease during polymerization, and such effects may influence the morphology of the deposition.

Polymer structures produced in a large-volume cell at low current density

In an attempt to assess the influence of the unfavorable electrode arrangement (and resulting non-uniform current distribution) of the ECAFM cell on the electrodeposited Ppy structures described in the preceding section, similar low current density experiments were conducted in a large-volume (ca. 100 cm^3) three-electrode cell. It should be noted, however, that the larger ratio of cell volume to working electrode area in these experiments will also reduce any effects due to depletion of monomer and decrease in pH that accompanies the electrodeposition (i.e., such effects would be of greater consequence in the ECAFM cell). Initial experiments were performed with a small Pt wire counter electrode to approximate the ratio of working electrode area to counter electrode area of the ECAFM cell. At a current density of 50 μA/cm^2, only very slow deposition of nodular Ppy occurred. No fiber-like Ppy structures could be detected. Thus, the fiber structures observed in the ECAFM cell is likely a consequence of the small volume cell and its far from optimum electrode arrangement.

However, during the course of these experiments, we did observe the interesting formation of tubular or vase-like structures of Ppy at higher deposition current and after long electrolysis times. For example, Fig. 4 shows SEM images of polypyrrole structures formed by Tiron-

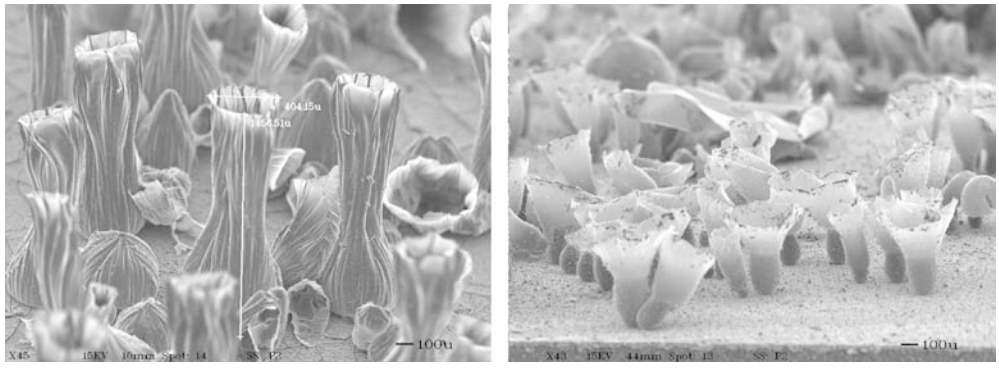

Fig. 4 SEM images of polypyrrole structures formed by a 3-h Tiron-mediated electrodeposition on Al 2024-T3 in the large-volume cell at a current density of 200 μA/cm^2. The deposition solution contained 0.1 M pyrrole and 0.1 M Tiron at pH 3 (*left*) and at pH 2 (*right*)

mediated electrodeposition on Al 2024-T3 in the large-volume cell at a current density of 200 $\mu A/cm^2$. The deposition solution contained 0.1 M pyrrole and 0.1 M Tiron at pH 3 (the left micrograph) and at pH 2 (the right micrograph). These structures are similar to those reported by Qu and co-workers [14, 15], although the conditions of formation in our work are rather different from theirs. Their work was conducted at rather high pyrrole concentration (typically 0.5 M) in the presence of a comparable concentration of surfactant (e.g., β-naphthalenesulfonic acid or sodium dodecylbenzenesulfonate) under either cyclic voltammetric scanning or controlled potential electrolysis. By varying experimental conditions, Qu and co-workers could generate a variety of structural shapes (including plates, bowls, cups, and vases), all resting on an underlying Ppy film [15].

The tubular structures observed in our work also grew from an underlying Ppy film of nodular morphology as determined by SEM (Fig. 5, left micrograph) in combination with EDS (results not shown). Visually, this underlying film was very non-uniform, certainly a consequence of non-uniform current distribution in the cell resulting from the use of a Pt microwire counter electrode. On average, our tubular structures appear somewhat larger in size and also somewhat more variable in size and shape than those reported by Qu et al. For example, the larger tubular structures in Fig. 4 (left micrograph) have a height of ca. 1400 μm and a diameter ca. 400 μm. The largest structures observed by Qu et al. were about one-third this size [15]. The size and geometry of our structures seem to be somewhat sensitive to small variations in the experimental conditions.

We believe the formation mechanism of the tubular structures observed in our work to be similar to that described by Qu et al. [14, 15]. They proposed a ''soap bubble'' mechanism, whereby the Ppy structures were templated by surfactant-stabilized gas bubbles generated by the catalyzed decomposition of water on the underlying Ppy film. Indeed, gas bubbles were observed during our electrolysis experiments, both on the underlying Ppy film and at the tips of the tubular structures. However, Tiron is not expected to be as good a surfactant as those used in the work of Qu et al., since polar groups are rather uniformly distributed around the benzene ring of Tiron. This may explain both the larger size and the variability of the structures we observe. A good surfactant might promote formation of small, uniform, stabilized ''soap bubbles'' which form smaller, more uniform templates for Ppy deposition, as observed in the work of Qu et al. [15].

Qu and co-workers reported that their microstructures did not form at potentials below 0.8 V (vs. SCE) using potentiostatic or potentiodynamic techniques. Interestingly, our structures are formed under galvanostatic conditions where the potential during the growth stage is ca. 0.52 V vs. Ag/AgCl, consistent with that reported previously at higher current density [6]. However, it should be noted that during the nucleation stage, lasting only a few seconds, the potential transiently reaches ca. 0.8 V. The higher potential is needed to initiate the Ppy deposition process, but a significantly lower potential will sustain Ppy film/structure growth.

Control experiments were conducted in which pTS replaced Tiron, all other conditions remaining the same. No Ppy deposition was observed for low current densities ($< 500\ \mu A/cm^2$) over the pH range 2–4. Ppy deposition occurred within a reasonable time interval only at a current density above ca. 800 $\mu A/cm^2$, in which case the deposited polymer exhibited only the nodular structure. No tubular structures were observed. As we reported previously, Ppy deposition on Al 2024-T3 in the absence of Tiron occurs at potentials several hundreds of millivolts more positive and is accompanied by substrate oxidation [6].

Another set of control experiments were conducted in which the Pt microwire counter electrode was replaced by a 4-cm×3-cm Pt plate arranged parallel to the working electrode, a more desirable electrode geometry for electrodepositions. Galvanostatic electrodeposition of Ppy at a current density of 200 $\mu A/cm^2$ from solutions containing 0.1 M pyrrole and 0.1 M Tiron at pH 3 led only to nodular-type Ppy films (Fig. 5), with no

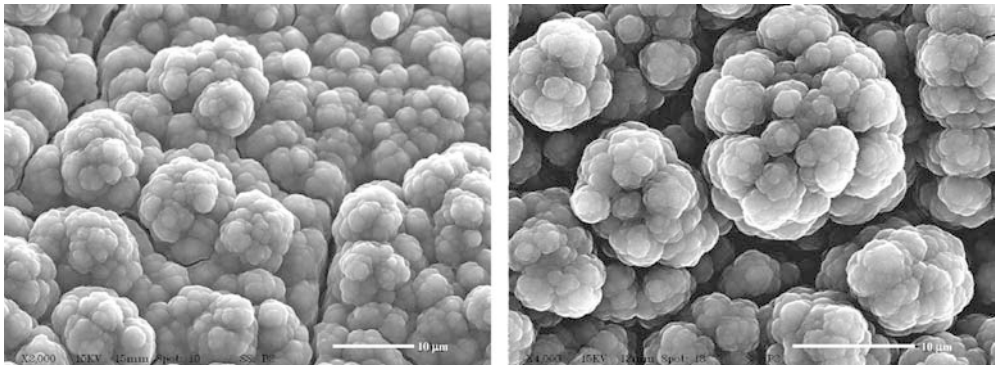

Fig. 5 SEM images of nodular polypyrrole structures formed by Tiron-mediated electrodeposition on Al 2024-T3 in the large-volume cell at a current density of 200 $\mu A/cm^2$. The deposition solution contained 0.1 M pyrrole and 0.1 M Tiron at pH 3. *Left*: Ppy film underlying the tubular structures formed with a Pt wire counter electrode. *Right*: only nodular Ppy was observed with a large counter electrode (Pt plate, 4-cm×3-cm). The figure on the right is at somewhat larger magnification (note length scales)

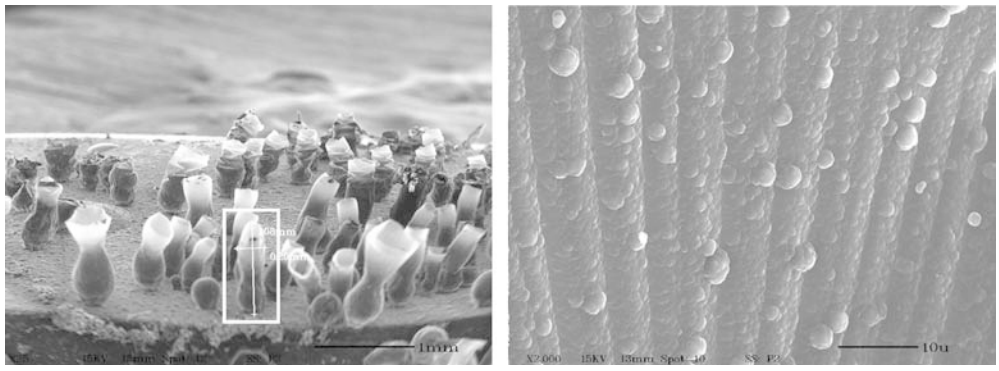

Fig. 6 SEM images of polypyrrole structures formed by a 3-h Tiron-mediated electrodeposition on Al 2024-T3 in the large-volume cell at a current density of 200 μA/cm^2. The deposition solution contained 0.1 M pyrrole and 0.1 M Tiron at pH 2. *Left*: low-resolution image. *Right*: high-resolution image of the side of the highlighted polypyrrole structure shown in the left image

formation of tubular structures. The potential during film growth was ca. 0.49 V, comparable to that observed with the Pt microwire counter electrode (0.52 V), but little or no gas bubble formation was observed with the Pt plate counter electrode. Nodular films were also obtained at higher current densities (to 1200 μA/cm^2). We conclude that non-uniform current density (and potential) distribution across the substrate surface plays a role in the formation of the tubular structures.

Conclusions

The question remains as to whether there is any relationship between the fiber-like structures observed in the ECAFM cell and the tubular structures observed in the large-volume cell. Conditions common to both observations are low current density, the presence of Tiron, and non-uniform current density. Otherwise, it is not clear that there is any relationship between the two types of structures. The star-burst type object in the SEM of Fig. 3 (left image) may be related to the tubular structures observed, for example, in Fig. 6. Both have overall widths on the order of a couple of hundred micrometers, and both have linear features associated with their morphology. A high magnification image of the side of one of the tubular structures is shown in Fig. 6. The walls of the tubular structure are composed of parallel fiber-like strands with a nodular sub-structure. The width of these strands is comparable to that of the fibers observed in the ECAFM cell, though clearly the sub-structure is different.

Interestingly, one-dimensional growth of Ppy with α–α' coupling has been proposed at current densities below ca. 300 μA/cm^2, whereas two-dimensional growth with α–β' coupling has been suggested for current densities above that value [13, 16, 17]. This cross-over current density of 300 μA/cm^2 is very close to the current density noted in our work, below which formation of fiber and tubular structures having one-dimensional character are favored. Further work is needed to elucidate the mechanism(s) of formation of these interesting structures.

Acknowledgements This work was supported by the Air Force Office of Scientific Research, grant nos. F49620-99-1-0283 and F49620-02-1-0398, North Dakota State University.

References

1. Tallman DE, Pae Y, Bierwagen GP (2000) Corrosion 56:401
2. He J, Johnston-Gelling V, Tallman DE, Bierwagen GP, Wallace GG (2000) J Electrochem Soc 147:3667
3. Johnston-Gelling V, Wiest MM, Tallman DE, Bierwagen GP, Wallace GG (2001) Prog Org Coat 43:149
4. Tallman DE, Spinks GM, Dominis AJ, Wallace GG (2002) J Solid State Electrochem 6:73
5. Tallman DE, He J, Johnston-Gelling V, Bierwagen GP, Wallace GG (2003) In: Zarras P, Stenger-Smith JD, Wei Y (eds) Electroactive polymers for corrosion control. (ACS symposium series 843) American Chemical Society, Washington, DC, pp 228–253
6. Tallman DE, Vang C, Wallace GG, Bierwagen GP (2002) J Electrochem Soc 149:C173
7. Tallman DE, Vang CK, Dewald MP, Wallace GG, Bierwagen GP (2003) Synth Met 135–136:33
8. Tallman DE, Dewald MP, Vang CK, Wallace GG, Bierwagen GP (2003) Curr Appl Phys (in press)
9. Yang XF, Tallman DE, Croll SG, Bierwagen GP (2002) Proceedings of the international conference on surface modification technologies. ASM International, Materials Park, Ohio, Indianapolis, IN, vol 15, p 119
10. Herrasti P, Ocon P (2001) Appl Surf Sci 172:276
11. Saidman SB, Bessone JB (2002) J Electroanal Chem 521:87
12. Suarez MF, Compton RG (1999) J Electroanal Chem 462:211
13. Appel G, Schmeisser D, Bauer J, Bauer M, Egelhaaf HJ, Oelkrug D (1999) Synth Met 99:69
14. Qu L, Gaoquan S (2003) Chem Commun 206
15. Qu L, Shi G, Chen F, Zhang J (2003) Macromolecules 36:1063
16. Schmeisser D, Naarmann H, Goepel W (1993) Synth Met 59:211
17. Schmeisser D, Bartl A, Dunsch L, Naarmann H, Gopel W (1998) Synth Met 93:43